BJUI
BJU International

MRI-safe robot for targeted transrectal prostate biopsy: animal experiments

Govindarajan Srimathveeravalli, Chunwoo Kim*, Doru Petrisor*, Paula Ezell, Jonathan Coleman†, Hedvig Hricak, Stephen B. Solomon and Dan Stoianovici*

*Department of Radiology, Memorial Sloan-Kettering Cancer Center, *URobotics Laboratory, Urology Department, Johns Hopkins University, and †Department of Surgery, Memorial Sloan-Kettering Cancer Center, New York, NY, USA*

Objectives

- To study the feasibility and safety of using a magnetic resonance imaging (MRI)-safe robot for assisting MRI-guided transrectal needle placement and biopsy in the prostate, using a canine model.
- To determine the accuracy and precision afforded by the use of the robot while targeting a desired location in the organ.

Materials and Methods

- In a study approved by the Institutional Animal Care and Use Committee, six healthy adult male beagles with prostates of at least 15 × 15 mm in size at the largest transverse section were chosen for the procedure.
- The probe portion of the robot was placed into the rectum of the dog, images were acquired and image-to-robot registration was performed. Images acquired after placement of the robot were reviewed and a radiologist selected targets for needle placement in the gland.
- Depending on the size of the prostate, up to a maximum of six needle placements were performed on each dog. After needle placement, robot-assisted core biopsies were performed on four dogs that had larger prostate volumes and extracted cores were analysed for potential diagnostic value.

Results

- Robot-assisted MRI-guided needle placements were performed to target a total of 30 locations in six dogs, achieving a targeting accuracy of 2.58 mm (mean) and precision of 1.31 mm (SD).
- All needle placements were successfully completed on the first attempt. The mean time required to select a desired target location in the prostate, align the needle guide to that point, insert the needle and perform the biopsy was ~ 3 min. For this targeting accuracy study, the inserted needle was also imaged after its placement in the prostate, which took an additional 6–8 min.
- Signal-to-noise ratio analysis indicated that the presence of the robot within the scanner bore had minimal impact on the quality of the images acquired.
- Analysis of intact biopsy core samples indicated that the samples contained prostatic tissues, appropriate for making a potential diagnosis.
- Dogs used in the study did not experience device- or procedure-related complications.

Conclusions

- Results from this preclinical pilot animal study suggest that MRI-targeted transrectal biopsies are feasible to perform and this procedure may be safely assisted by an MRI-safe robotic device.

Keywords

MRI, robotic assistance, prostate, biopsy

Introduction

Prostate cancer (PCa) is a complex and heterogeneous disease with a wide diversity in volume, grade and sites of cancer within the gland, all of which are associated with an individual's risk of disease progression [1]. Biopsy findings are the most critical component to determine the course of clinical management, which ranges from active surveillance for low grade tumours, to surgery or radiation for cancers that are found to be more aggressive [2,3]. TRUS-guided biopsy is commonly used in the diagnosis and evaluation of the disease [4,5]. While this technique offers the convenience of being performed under local anaesthesia in a clinic-office setting, a limitation of this method is that grey-scale ultrasonography provides limited tumour-specific imaging information regarding location or amount of tumour; therefore, biopsies performed using this method generally do not specifically target lesions. Ultrasonogaphy-guided biopsies are performed to sample the gland systematically according to a schema, but are cancer 'blind' and, as a result, can have low sensitivity and poor negative prediction rates [6–8]. Additionally, since PCa is a heterogeneous multifocal disease, untargeted biopsies can

BJU International © 2013 BJU International | doi:10.1111/bju.12335
Published by John Wiley & Sons Ltd. www.bjui.org

sometimes detect small, isolated cancer foci which can be associated with clinically insignificant tumours (i.e. Gleason grade 6, <0.5 mL) and which may misrepresent the true risk of disease [9]. Finally, with the variability in manual TRUS-guided techniques, sampling strategies may lead to clustering in certain regions of the gland and under-sampling in larger glands which can miss regions that contain clinically significant tumours [10]. Both over-diagnosis of clinically insignificant cancer and under-diagnosis of potentially lethal cancers exist in the screening population [9], which means that the technology currently used for prostate biopsy creates uncertainty in the field and is a barrier to appropriate stratified management [11].

Among imaging methods, MRI provides the highest spatial and contrast resolution on prostate anatomy [12]. MRI of the prostate with techniques, such as T2-weighted imaging, diffusion-weighted imaging and magnetic resonance spectroscopic imaging, provide additional measures for detecting cancer-suspicious regions and have higher specificity, allowing improved determination of the type and nature of the lesion [13–18]. In particular, there is fresh evidence that multiparametric MRI can identify low suspicion lesions and therefore can be used as a test for high grade disease [19], and that transperineal MRI-guided biopsy can provide better diagnostic results than transperineal template biopsies [20]. The limitations of magnetic resonance spectroscopic imaging that limit wider adoption include a lack of established criteria to distinguish and identify cancerous lesions from BPH and prostatitis in the transitional zone, large voxel size leading to averaging of signal and lack of resolution [21]. Imaging and PCa image biomarkers still require further validation and have recognized limitations, including the potential for false-positive and false-negative results [22]. Although not perfect and still under development, using MRI findings to target the regions that have the highest probability of being cancer has great potential.

Ultrasonography– MRI image fusion was developed to combine the strengths of the two imaging techniques to provide better visualization for targeting suspicious lesions [23,24]. TRUS-fusion-guided biopsy has been extensively evaluated in patients; Sonn et al. [25] report the benefits of combining the soft tissue visualization of MRI and the convenience of US-guided office-based biopsy, Kuru et al. [26] and Mark et al. [27] report the benefits of improved targeting and therefore reducing the number of biopsies taken, and Vourganti et al. [28] suggest that it may be an ideal tool for the diagnosis of suspicious lesions on MRI that were negative on previous TRUS biopsies.

The patient has to undergo imaging twice to perform fusion-imaging-guided targeting (MRI followed by TRUS) which is a limitation of this technique. As an alternative approach, several groups [29–43] have investigated using robotic assistance to perform MRI-guided prostate biopsies within the scanner itself. The strong magnetic field of the MRI precludes the use of many metallic materials, limiting the choice of construction materials to build the robot and imposes constraints on the types of actuators that can be used within the magnet without affecting the image quality. This makes construction of devices that can be safely operated in the MRI a challenge.

Unlike TRUS-fusion biopsies which exclusively use a transrectal approach, a transperineal, transrectal or transgluteal approach can be used to place needles in the prostate using robotic assistance. Multiple groups [29–34,42] have developed robotic systems that assist needle placement in the prostate using a transperineal approach. The robot designed by Tokuda et al. [29] and Seifabadi et al. [30] functions as a master–slave teleoperated system and was evaluated pre-clinically using phantom models. Van den Bosch et al. [31] constructed their robot as a semi-manual needle positioning mechanism and the robot was used to plant four gold fiducial markers in a single patient. Muntener et al. [32,36] and Stoianovici et al. [33] developed a MRI-stealth robot for transperineal needle access of the prostate. Long et al. [42] performed an evaluation of their robot using a deformable phantom model; however, as reported, this robot cannot be used within the MRI scanner. Ho et al. [44] also reported on a non-MRI-compatible but US-guided robotic platform using the transperineal approach for performing biopsies and therapy that has been successfully evaluated through human patient clinical trials [45]. Apart from the transperineal approach, the study by Zangos et al. [34] is the only reported evaluation of the transgluteal approach. They used a remote-controlled robot to successfully perform prostate biopsies in a cohort of 20 patients. Finally, Yakar et al. [35] report using a transrectal approach and a remote-controlled robot to guide biopsies safely in a cohort 10 patients. Thorough reviews, discussing the engineering and construction of these different robots and their clinical application, are provided by Cleary et al. [46] and Futterer et al. [47].

The above-mentioned studies establish the early feasibility and safety of using robotic assistance for placing needles and guiding biopsies within the MRI scanner. With the exception of the US-guided robotic system reported by Ho et al. [45], the majority of the reviewed literature using the transperineal approach was developed for placing brachytherapy seeds and not for performing biopsies or therapy. There are fewer MRI-guided robotic systems supporting the transrectal approach that is currently commonly used for TRUS biopsies in the prostate. A manually operated transrectal biopsy device was investigated by Susil et al. [37] in a closed-bore 1.5T scanner. This incorporated an imaging coil, special position tracking coils, and a needle guide. They showed improved cancer detection in MRI-guided biopsies when the

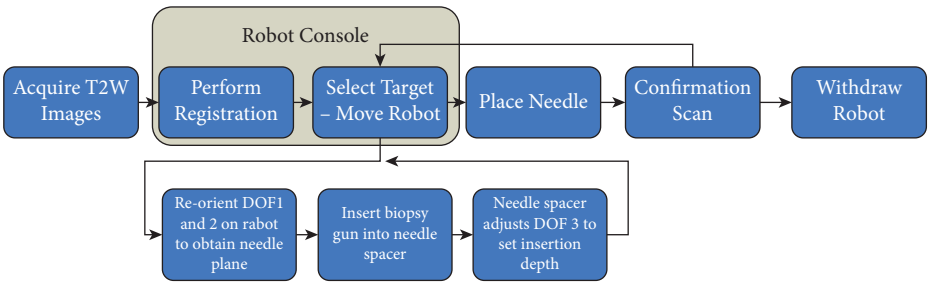

Fig. 1 Workflow adopted for placing needles after placing robot in the rectum of each dog. T2W, T2-weighted.

MRI-guided biopsy was not performed immediately after the TRUS-guided biopsy [38]. Several versions of this device have been reported in literature, two versions of which can use a curved needle path [39,40]; however, such manually operated devices can be difficult to operate because of the limited access within the MRI scanner and numerous table movements may be required to access the patient. An actuated device was recently reported from the Nijmegen Medical Centre in the Netherlands [41]. This was the first actuated MRI-guided transrectal biopsy device to be tested clinically [35]. Early results from their study provide positive evidence of the feasibility and safety of using the transrectal approach for needle placement and biopsies in the prostate. This device is remotely operated and, as reported in the literature, did not feature image-to-robot registration which would have allowed automatic re-positioning of the robot based on selected targets in the prostate.

Taking these factors into consideration, we report the pre-clinical canine model testing of an MRI-guided MRI-safe (American Society for Testing and Materials, ASTM F2503) robot that was developed for assisting transrectal prostate biopsy in the MRI scanner [43]. The software developed with the robot allows registration of the robot with the image set, allowing automatic needle-guidance based on physician selected targets. Compared with manually actuated [37] or master–slave robots [41], this approach could reduce the cognitive and dexterity demand on the physician during initial needle placement. This software–robot combination can be operated within the scanner bore and may therefore minimize the number of times the patient/table has to be moved while performing MRI-guided prostate biopsies.

Materials and Methods

Study Protocol

After obtaining Institutional Animal Care and Use Committee approval, seven male beagles were used to perform the study. The dogs were acquired when they were ~ 9–14 months of age, weighing between 9 and 11 kgs. The dogs were screened using ultrasound imaging and only those with a prostate that was at least 15 × 15 mm at the largest cross section were selected for use in the study. All the dogs used in the study recovered after the procedure, and were placed in a week-long observation period to document any unintended morbidities arising as a result of robot-assisted needle placements. After the observation period, an orchiectomy was performed and the dogs were adopted.

The study was conducted using a 3 Tesla Signa HDx MRI scanner (GE Healthcare Systems, Schenectady, NY, USA) with an eight-channel torso coil and the endorectal coil mounted on the end effector of the robot. Both coils were used in tandem to acquire all the images used in the study. The experimental protocol and workflow used for collecting the presented data is shown in Fig. 1. Before the MRI scan, each dog was sedated with an i.m. injection of acepromazine (0.05 mg/kg) and buprenorphine (0.01 mg/kg), induced with i.v. administered propofol (6 mg/kg). After intubation the dogs were moved to the scanner table and placed in the prone position head first in the scanner, and maintained on isoflurane (1–3%) and given i.v. fluids and cefazolin (22 mg/kg). Foam pads and towels were used to elevate the pelvis of the animal at a ~20–30 degree angle, which facilitated the placement of the robot into the rectum of the animal. The pelvic region of the dog was then imaged without the robot using a T2-weighted fast spin echo sequence (TE:102 TR:3200 field of view [FOV]: 20 Echo train length:24 ST: 3 mm NEX: 3 Matrix: 256 × 192 acquired in the axial and the sagittal planes). These images were examined by the radiologist to determine any obstructions in the rectum or unusual anatomy to decide the suitability of the dog for the study. The rectum of the dog was then manually dilated, lubricated with surgical lube and 2% topical lidocaine solution, and the rectal probe portion of the robot was placed into the dog's rectum. T2-weighted fast spin echo images (TE:102 TR:4500 FOV: 20 Echo train length:12 ST:2 mm NEX: 2 Matrix: 256 × 256 acquired in the axial plane) were used to localize the robot inside the dog's rectum and subsequently to perform image-to-model registration of the robot. This image series was also used to determine suitable locations for needle placement and biopsy. Target selection and needle placements followed this, and immediately after each needle placement, the prostate and the adjacent rectal region was scanned (T2-weighted fast spin echo, TE:102 TR:4500 FOV: 20 Echo train length:12 ST:2 mm NEX: 2 Matrix: 256 × 256 acquired in the axial plane) to acquire the needle path to the target location. Upon completion of the study the robot was removed from the dog's rectum and the pelvic region was

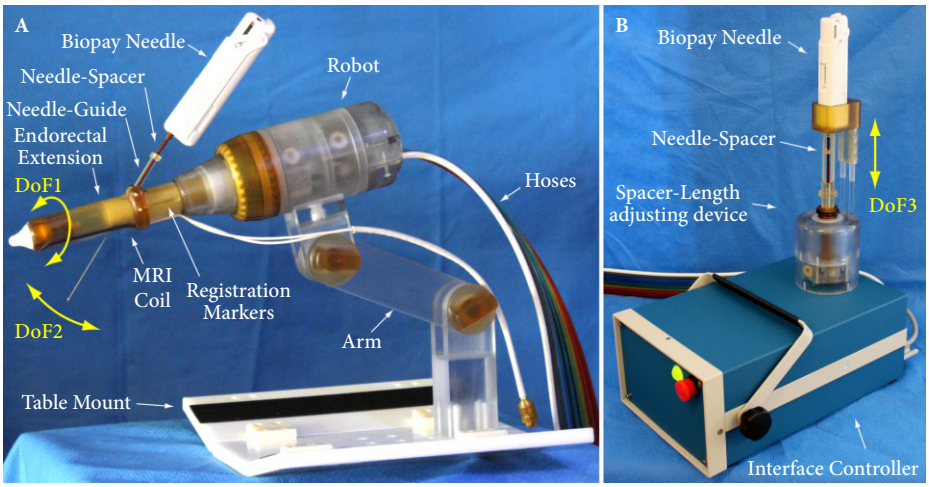

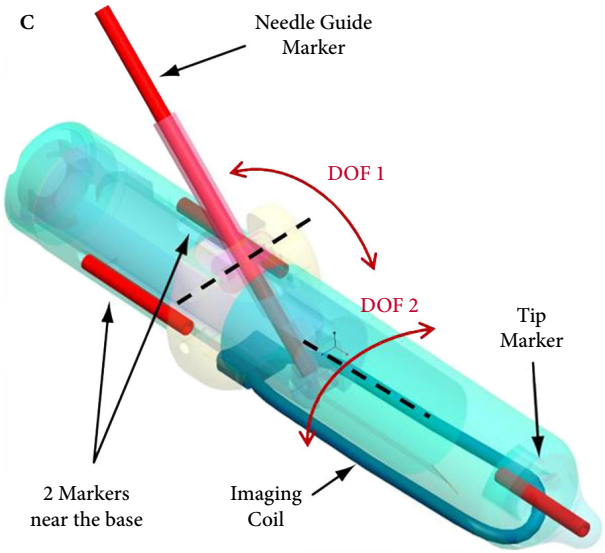

Fig. 2 **A**, The needle guide on the robotic probe features two DoF that allows placement of the needle in a selected plane in three-dimensional space. **B**, Third DoF for setting the depth of needle insertion is located on an interface controller box that also houses the control and electronics for the robot. **C**, A more detailed representation of the DoF present on the robotic probe. The two rotational DoF setting the plane of the needle guide are represented by the red arrows and the axis of rotation is depicted by the black dashed lines.

imaged to ascertain any incidental trauma, clinically significant rectal bleeding or damage to sensitive structures near the prostate. After imaging confirmed the absence of clinically significant bleeding, each dog received s.c. injections of carprofen (4.4 mg/kg) before recovery from anaesthesia. All dogs were given cephalexin for 7 days, buprenorphine for 3 days and carprofen for 4 days after the procedure.

Transrectal Biopsy Robot

An MRI-safe (ASTM- F2503) robot was developed. A technically detailed description of the construction and the functioning of the robot is provided by Stoianovici et al. [43]. The robot was constructed using non-metallic materials, and uses pneumatic actuation and optical sensors. The robot is electricity-free. The joints of the robot were actuated using MRI-compatible stepper motors specifically developed for the robot [48]. The robot presents three degrees of freedom (DoF), two used to orient the needle guide that is present on the endorectal extension of the robot, and the other to adjust the insertion depth of the needle (Fig. 2). The endorectal probe portion of the robot features an MRI coil, and a set of four registration markers filled with MRI contrast (Beekley Corp., Bristol, CT, USA). The markers were used to register the robot to MRI space by image-to-model registration. Image-to-model registration and navigation algorithms were implemented in custom C++ module integrated into the Amira (Visage Imaging, San Diego, CA, USA) visualization software. These are also used to load MRI images and perform target selection (Fig. 3). The robotic system and software is currently unapproved for human use and an Investigational Device Exemption (IDE) application is pending review for commencing clinical studies in human patients.

Needle Placement Procedure

Depending on the relative size of the dog's prostate, up to six needle placements (including subsequent biopsies where

Fig. 3 Screenshot capture of the software used to perform registration. The two images represent results seen from two different three-dimensional views obtained following robot to image registration using a single dataset. The computer-aided design models representing the fiducial markers on the robot can be seen (red) overlaid with the isosurface extracted from the images (tan). The needle path (indicated by the solid arrow) calculated after performing inverse kinematics can be seen with the tip pointing at the target (indicated by the dashed arrow). The body of the robot is not indicated in this figure.

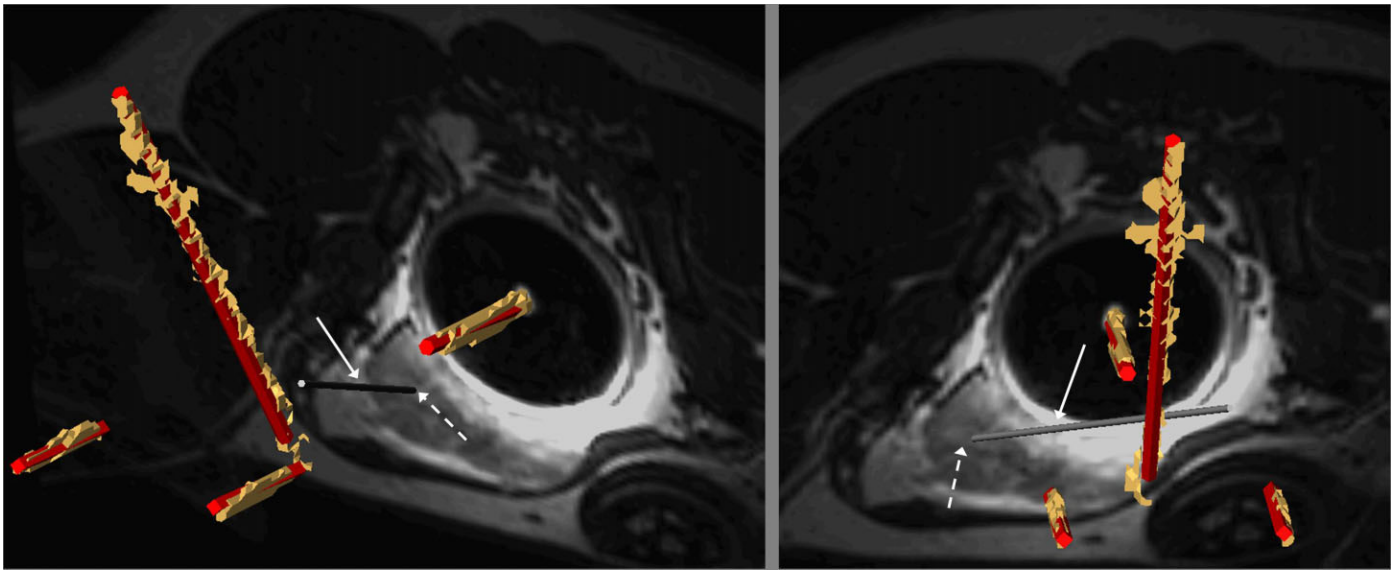

possible) were performed on each dog. As there were no obvious tumours to decide the desired target locations, suitable locations were chosen by a trained interventional radiologist who chose locations equally on either side of the urethra in the peripheral and central aspects of the organ. Using the registration mapping and inverse kinematics algorithms, the selected location was converted to robot joint coordinates, and the robot was automatically re-oriented to point the needle guide to the target location. An 18-G, 175-mm fully automatic biopsy needle (Invivo MR18G175, Pewaukee, WI, USA) was used to obtain the samples. Prostate biopsy was performed on four of the six dogs, and the acquired cores were analysed for quantity and quality of the sampled tissue. The dogs with the largest gland volumes were used as candidates to perform the biopsies. The biopsy samples were stored in 10% neutral buffered formalin before submission for histopathology analysis to estimate the quantity of prostate tissue in the biopsy core and its potential diagnostic value.

Data Analysis

The targeting error was calculated based on the target image set on which selection of the location in the prostate for the needle tip was made, and the image set was acquired after each needle placement in the selected location (needle image set). To calculate the accuracy of placements, these two image sets were automatically registered by their common reference frame. After this, the image coordinates of the selected target (${}^1x_i$) from the target image set and the centre of the image artifact caused by the needle tip (${}^2x_i$) from the needle image set was measured (Fig. 4). Targeting errors were then calculated as the distance between two coordinates, $\varepsilon = |{}^1x_i - {}^2x_i|$. The accuracy and precision of targeting were then calculated as mean and SD values of the distance, respectively. It must be noted that an elongated metallic object like a needle can cause imaging artifact in two directions when imaged using MRI. The needle can appear both longer or thicker than its actual size, and this artifact in imaging is dependent on the orientation of the needle relative to B_0 of the magnet and the frequency encoding direction [49,50]; therefore, in addition to recording the error between the selected target point and the apparent needle tip location in the co-registered image series, the number of slices through which the needle artifact extended beyond the target slice was also recorded. This study was performed with imaging acquired at a minimum slice thickness of 2.0 mm, which then represents the lower limit for calculation of the targeting error.

To determine the impact of the robot's presence on the quality of images acquired, signal-to-noise ratio (SNR) calculations were performed using the axial T2 images acquired before and immediately after placing the robotic probe in the dog's rectum. The image slice where the prostate could be observed at its largest cross section was identified in the pre- and post-robot placement image sets and used for analysis. Two circular regions of interest, 25 mm^2 in area, were created and one was placed within the prostate gland and the other was placed in the background of the image. The mean and SD values of the signal at these two regions of interest were

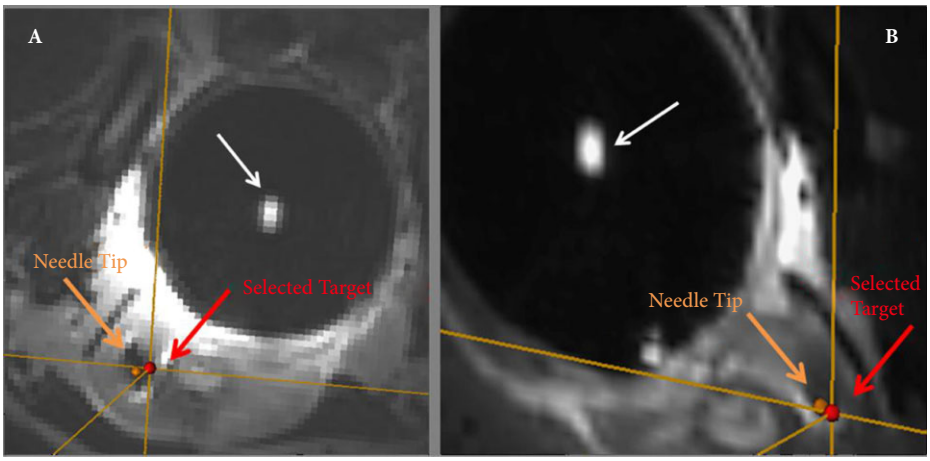

Fig. 4 Images showing the selected target location (red dot) and the centre of the needle tip as seen on imaging (orange dot). The fiducial marker on the robot's axis can be seen at the centre of the image (white arrow). As a reference for size, this marker is 2.5 mm in diameter.

acquired and stored as $\mu_{prostate}$ and as $\mu_{background}$, respectively. The SNR was then calculated separately for each image set using the formula SNR = $(0.66^{*}\mu_{prostate} / \sigma_{background})$. The SNR for the post-insertion image was then normalized with the SNR of the pre-insertion image considered to be the baseline value.

Results

A total of 30 MRI-guided needle placements (Fig. 5) were carried out in six dogs (dog 1: six, dog 2: five, dog 3: five, dog 4: six, dog 5: four and dog 6: four needle placements), one dog was omitted from the study as it had consumed bedding material that obstructed the rectum and had caused bleeding, the robot was never placed in this dog. The resulting data indicated that a targeting accuracy of 2.58 mm (mean targeting error) and precision of 1.31 mm (SD of error) were achieved. The method used for the calculation of needle placement accuracy and precision is reported in the data analysis section. The minimum recorded placement error was 0.75 mm and the maximum recorded placement error was 5.44 mm. The artifact caused by the needle in the post-placement images extended to a mean of 0.6 slices with a SD of 1.10 slices in the 30 image sets analysed. All needle placements were performed within a single attempt. That is, it was possible to place a needle at a target location without having to reposition the robot more than once, and the needle guide on the robot provided unfettered access such that multiple insertions and withdrawals were not required to insert the needle into the gland. The procedure time for dogs 2–6 was kept fixed at 3 h, which included the set-up time, total imaging time and time taken for multiple needle placements and biopsies. The mean time required to select a target, move the robot to the target location and place the needle was ~ 3 min. After performing needle placement, the needle was imaged at the target location which took an additional 6–8 min. The normalized SNR from all the experiments after insertion of the robot was calculated at a mean value of 9.99 with a SD of 2.88. One of the reasons for this dramatic increase from the pre-insertion values could be the use of the endorectal coil present on the robot probe which generated significant, additional signals close to the prostate gland.

Fig. 5 Reformatted sagittal image acquired after the insertion of the needle to a target location. The portion of the rectum dilated by the robot's probe can be seen as the dark region with an absent MRI signal in the centre of the image. The boundary of the prostate has been outlined using the white dashed line. The boundary of the needle's body (signal void caused by presence of metal) has been outlined using a solid white line and the needle tip is indicated by the arrow.

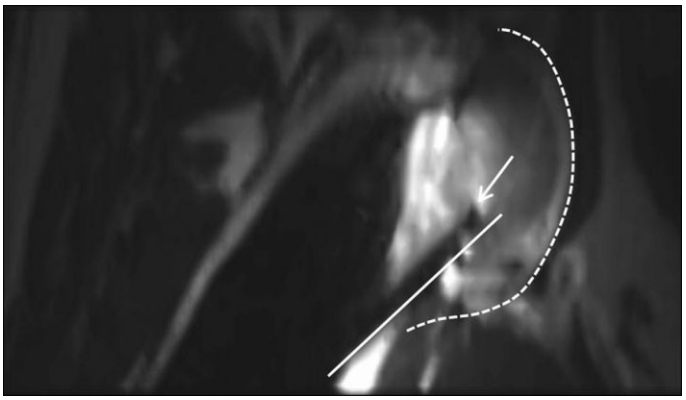

Healthy dogs were used to conduct our study, and therefore, there were no specific lesions observable in MRI to target the biopsies. The biopsies were therefore directed to locations in the prostate that could safely accommodate the whole notch of the biopsy gun (15 mm). A total of seven biopsy samples were obtained from four dogs. The number of biopsy samples taken was restricted by the relatively smaller size of the canine prostate and the location of prostate. Core samples were obtained from all biopsies. Analysis of intact core samples indicated that the cores contained normal prostatic tissue sufficient for making a potential diagnosis if necessary.

None of the dogs in the study experienced complications as a result of needle placements or the insertion of the robot in the rectum. Images acquired after the removal of the robot did not indicate any injury to the rectum or clinically significant bleeding. There was some localized swelling and oedema, which is expected where there have been multiple needle placements. The dogs were given antibiotics and palliative care, recovering within 1–2 days without signs of rectal discomfort.

Discussion

This pre-clinical study establishes the feasibility of image-guided automatic needle positioning for performing MRI-guided robot-assisted transrectal prostate biopsies. Targeting experiments were based on MRI images that include needle point artifacts. As a result of these inherent measurement errors, the precision and accuracy results may actually be superior to those that we could measure. In any case, the size of a clinically significant PCa tumour is 0.5 mL, corresponding to a spherical shape of a ~5 mm radius. As the mean targeting accuracy was <5 mm, these results suggest that the device is sufficiently accurate to guide needle placement for prostate biopsy.

The MRI-safe biopsy device may provide an instrument for correlating a MRI abnormality with a pathological finding from the biopsy samples, and increasing the sensitivity of biopsy. The present study also indicates that the presence of the robot does not seem to qualitatively affect the spectra of a healthy prostate. This could make magnetic resonance spectroscopic imaging-directed biopsies possible in the future.

The registration of the robot with the MRI scanner allows automatic navigation to target locations selected by the physician using a simple point-and-click graphical user interface. The workflow of our robot requires only a single image series for registration and targeting, thereby minimizing the number of times the robot has to be moved or re-imaged.

Presently, only two studies have explored the feasibility of using robotic assistance and MRI guidance for performing prostate biopsies in human patients. Zangos et al. [34] report results from performing needle placements using a transgluteal approach, and Yakar et al. [35] report the only study performed using the transrectal approach. Both studies indicate positive results, and the latter study confirms the feasibility and the safety of using a robot in human patients to place needles in the prostate using the transrectal approach; however, the system used by Yakar et al. [35] for their study was remotely operated, without image-to-robot registration and so the accuracy of positioning the needles was contingent on the experience of the physician remotely operating the robot and therefore may not be a true indicator of the targeting acuity achievable when using a robotic needle positioning system. In any case, this represents a very promising technology which is undergoing continuing development and testing. TRUS-image-fusion- guided biopsy is another navigation technique that has achieved widespread clinical use and value. Ukimura et al. [51] report typical targeting errors in the region of 2.35–2.92 mm when performing image-fusion-guided biopsies in a phantom model. The targeting error values from our experiments are in a similar range and therefore we can conclude our approach was equivalent to image-fusion guidance for biopsies in a pre-clinical setting.

The present study evaluated needle placement using a transrectal approach. Currently, the majority of biopsies are extracted using this approach with ultrasonography guidance, with good safety profiles and minimal morbidity [52]; however, the rise of antibiotic-resistant strains of bacteria and the associated risk of infection after TRUS biopsies has become a cause for concern about the continued use of this approach for the diagnosis of PCa [53,54]. These factors have motivated research into the use of transperineal template biopsy as an alternative approach, with a lower risk of infection and lower prophylaxis requirements [55]. This is an important factor which may necessitate a re-design of our robot to include a transperineal needle approach when translating this to clinical use.

Certain shortcomings remain in the present study. First, it is a preliminary study performed on a canine model which cannot capture all the challenges of performing MRI-guided biopsies on human patients under conscious sedation. Second, the dogs used for this study were healthy, and therefore, there was no obvious lesion to target for needle placements. Because of this, the targets were selected empirically based on anatomical locations with respect to prostate and the urethra. This reduces the objectivity of the measurements. The small size of the dog's prostate also limited the biopsies samples that could be withdrawn and analysed. Finally, the lack of a control group (manual intervention) limits comparison of the time taken, number of needle passes used and accuracy measures of the robot with equivalent manual intervention. The accuracy measures of the study were taken from the post-needle placement images which are prone to artifactual errors, and the slice thickness used for the study was kept at 2.0 mm. To determine the positioning accuracy of the robot objectively, a concurrent study was performed using a gelatin phantom with CT imaging at 0.625-mm slice thickness. This study was used to verify the spatial accuracy (1.10 mm) and precision (0.33 mm) of the robot, independent of the prostate and MRI [49].

The practice of MRI-guided transrectal biopsy in itself presents some additional issues that require consideration. Transrectal biopsy risks sepsis and with the increased incidence of drug-resistant bacteria, the associated morbidity needs to be addressed, either through improved prophylaxis or

by protocol changes to reduce the introduction of bacteria into the prostate gland. This risk may also be reduced by using our robot with a transperineal approach which may be evaluated in a follow-up study. While MRI can provide superior imaging results, the expense of this imaging technique and its availability limits its use in the traditional clinic-office settings where a large proportion of ultrasonography-guided biopsies are performed; however, there is value in using multimodal MRI and robotics to assist biopsies which will improve imaging–pathology correlation, so these results may eventually improve the value of MRI as a stand-alone diagnosis tool.

In addition to diagnosis, a potential benefit of the use of this robot in the future would be to assist MRI focal-guided therapies for PCa or to follow patients on active surveillance. Biopsy mapping with this device would allow accurate guidance of treatment needles or optical fibres back into the cancer-containing regions of the gland to perform focal therapy of the lesion and surrounding tissue. MR thermography can potentially be used to monitor the progress of the ablation and, upon completion, diffusion-weighted imaging could be used to confirm the efficacy of such treatment.

Acknowledgement

This project was supported by award number W81XWH0810221 from the Prostate Cancer Research Program of the US Department of Defense. The content is solely the responsibility of the authors and does not necessarily represent the official views of the Prostate Cancer Research Program or the Department of Defense.

Conflict of Interest

None declared.

References

1 **Troyer DA, Mubiru J, Leach RJ, Naylor SL.** Promise and challenge: Markers of PCa detection, diagnosis and prognosis. *Dis Markers* 2004; 20: 117–28

2 **Bastian PJ, Carter BH, Bjartell A et al.** Insignificant PCa and active surveillance: from definition to clinical implications. *Eur Urol* 2009; 55: 1321–30

3 **Dall'era MA, Albertsen PC, Bangma C et al.** Active surveillance for PCa: a systematic review of the literature. *Eur Urol* 2012; 6: 976–83

4 **Yacoub JH, Verma S, Moulton JS, Eggener S, Aytekin O.** Imaging-guided prostate biopsy: conventional and emerging techniques. *Radiographics* 2012; 32: 819–37

5 **Djavan B, Milani S, Remzi M.** Prostate biopsy: who, how and when. An update. *Can J Urol* 2005; 12 (Suppl 1): 44–8; discussion 99–100

6 **Rocco B, de Cobelli O, Leon ME et al.** Sensitivity and detection rate of a 12-core trans-perineal prostate biopsy: preliminary report. *Eur Urol* 2006; 49: 827–33

7 **Terris MK.** Sensitivity and specificity of sextant biopsies in the detection of PCa: preliminary report. *Urology* 1999; 54: 486–9

8 **Master VA, Chi T, Simko JP, Weinberg V, Carroll PR.** The independent impact of extended pattern biopsy on PCa stage migration. *J Urol* 2005; 174: 1789–93

9 **Kelloff GJ, Choyke P, Coffey DS.** Challenges in clinical PCa: role of imaging. *AJR Am J Roentgenol* 2009; 192: 1455–70

10 **Han M, Kim C, Chang D et al.** Geometric Evaluation of Systematic Transrectal Ultrasound-Guided Prostate Biopsy. *J Urol* 2012; 188: 2404–9

11 **Stoianovici D.** Technology advances for prostate biopsy and needle therapies. *J Urol* 2012; 188: 1074–5

12 **Hricak H, Choyke PL, Eberhardt SC, Leibel SA, Scardino PT.** Imaging prostate cancer: a multidisciplinary perspective. *Radiology* 2007; 243: 28–53

13 **Soylu FN, Eggener S, Oto A.** Local staging of PCa with MRI. *Diagn Interv Radiol* 2012; 18: 365–73

14 **Mazaheri Y, Shukla-Dave A, Muellner A, Hricak H.** MRI of the prostate: clinical relevance and emerging applications. *J Magn Reson Imaging* 2011; 33: 258–74

15 **Shukla-Dave A, Hricak H, Ishill N et al.** Prediction of PCa recurrence using magnetic resonance imaging and molecular profiles. *Clin Cancer Res* 2009; 15: 3842–9

16 **Zakian KL, Shukla-Dave A, Ackerstaff E, Hricak H, Koutcher JA.** 1H magnetic resonance spectroscopy of PCa: biomarkers for tumor characterization. *Cancer Biomark* 2008; 4: 263–76

17 **Kobus T, Hambrock T, Hulsbergen-van de Kaa CA et al.** In vivo assessment of PCa aggressiveness using magnetic resonance spectroscopic imaging at 3 T with an endorectal coil. *Eur Urol* 2011; 60: 1074–80

18 **Swindle P, McCredie S, Russell P et al.** Pathologic characterization of human prostate tissue with proton MR spectroscopy. *Radiology* 2003; 228: 144–51

19 **Yerram NK, Volkin D, Turkbey B et al.** Low suspicion lesions on multiparametric magnetic resonance imaging predict for the absence of high-risk prostate cancer. *BJU Int* 2012; 110 (11 Pt B): E783–8

20 **Kasivisvanathan V, Dufour R, Moore CM et al.** Transperineal magnetic resonance image targeted prostate biopsy versus transperineal template prostate biopsy in the detection of clinically significant prostate cancer. *J Urol* 2013; 189: 860–6

21 **Nayyar R, Kumar R, Kumar V, Jagannathan NR, Gupta NP, Hemal AK.** Magnetic resonance spectroscopic imaging: current status in the management of prostate cancer. *BJU Int* 2009; 103: 1614–20

22 **Afaq A, Koh DM, Padhani A, van As N, Sohaib SA.** Clinical utility of diffusion-weighted magnetic resonance imaging in prostate cancer. *BJU Int* 2011; 108: 1716–22

23 **Xu S, Kruecker J, Turkbey B et al.** Real-time MRI-TRUS fusion for guidance of targeted prostate biopsies. *Comput Aided Surg* 2008; 13: 255–64

24 **Singh AK, Kruecker J, Xu S et al.** Initial clinical experience with real-time transrectal ultrasonography-magnetic resonance imaging fusion-guided prostate biopsy. *BJU Int* 2008; 101: 841–5

25 **Sonn GA, Natarajan S, Margolis DJ et al.** Targeted biopsy in the detection of prostate cancer using an office based magnetic resonance ultrasound fusion device. *J Urol* 2013; 189: 86–91

26 **Kuru TH, Roethke MC, Seidenader J et al.** Critical evaluation of MRI-targeted TRUS-guided transperineal fusion biopsy for detection of prostate cancer. *J Urol* 2013; doi: 10.1016/j.juro.2013.04.043. [Epub ahead of print]

27 **Marks L, Young S, Natarajan S.** MRI-ultrasound fusion for guidance of targeted prostate biopsy. *Curr Opin Urol* 2013; 23: 43–50

28 **Vourganti S, Rastinehad A, Yerram NK et al.** Multiparametric magnetic resonance imaging and ultrasound fusion biopsy detect prostate cancer in patients with prior negative transrectal ultrasound biopsies. *J Urol* 2012; 188: 2152–7

29 **Tokuda J, Song SE, Fischer GS et al.** Preclinical evaluation of an MRI-compatible pneumatic robot for angulated needle placement in

transperineal prostate interventions. *Int J Comput Assist Radiol Surg* 2012; 7: 949–57

30 **Seifabadi R, Song SE, Krieger A et al.** Robotic system for MRI-guided prostate biopsy: feasibility of teleoperated needle insertion and ex vivo phantom study. *Int J Comput Assist Radiol Surg* 2012; 7: 181–90

31 **van den Bosch MR, Moman MR, van Vulpen M et al.** MRI-guided robotic system for transperineal prostate interventions: proof of principle. *Phys Med Biol* 2010; 55: N133–40

32 **Muntener M, Patriciu A, Petrisor D et al.** Transperineal prostate intervention: robot for fully automated MR imaging–system description and proof of principle in a canine model. *Radiology* 2008; 247: 543–9

33 **Stoianovici D, Song D, Petrisor D et al.** "MRI Stealth" robot for prostate interventions. *Minim Invasive Ther Allied Technol* 2007; 16: 241–8

34 **Zangos S, Melzer A, Eichler K et al.** MR-compatible assistance system for biopsy in a high-field-strength system: initial results in patients with suspicious prostate lesions. *Radiology* 2011; 259: 903–10

35 **Yakar D, Schouten MG, Bosboom DG, Barentsz JO, Scheenen TW, Fütterer JJ.** Feasibility of a pneumatically actuated MR-compatible robot for transrectal prostate biopsy guidance. *Radiology* 2011; 260: 241–7

36 **Muntener M, Patriciu A, Petrisor D et al.** Magnetic resonance imaging compatible robotic system for fully automated brachytherapy seed placement. *Urology* 2006; 68: 1313–7

37 **Susil RC, Menard C, Krieger A et al.** Transrectal prostate biopsy and fiducial marker placement in a standard 1.5T magnetic resonance imaging scanner. *J Urol* 2006; 175: 113–20

38 **Singh AK, Krieger A, Lattouf JB et al.** Patient selection determines the prostate cancer yield of dynamic contrast-enhanced magnetic resonance imaging-guided transrectal biopsies in a closed 3-Tesla scanner. *BJU Int* 2007; 101: 181–5

39 **Susil RC, Krieger A, Derbyshire JA et al.** System for MR image-guided prostate interventions: canine study. *Radiology* 2003; 228: 886–94

40 **Krieger A, Susil RC, Menard C et al.** Design of a novel MRI compatible manipulator for image guided prostate interventions. *IEEE Trans Biomed Eng* 2005; 52: 306–13

41 **Schouten MG, Ansems J, Renema WK, Bosboom D, Scheenen TW, Futterer JJ.** The accuracy and safety aspects of a novel robotic needle guide manipulator to perform transrectal prostate biopsies. *Med Phys* 2010; 37: 4744–50

42 **Long JA, Hungr N, Baumann M et al.** Development of a novel robot for transperineal needle based interventions: focal therapy, brachytherapy and prostate biopsies. *J Urol* 2012; 188: 1369–74

43 **Stoianovici D, Kim C, Srimathveeravalli G et al.** MRI-Safe Robot for Transrectal Prostate Biopsy. *IEEE/ASME Trans Mechatron* 2012

44 **Ho H, Yuen JS, Cheng CW.** Robotic prostate biopsy and its relevance to focal therapy of prostate cancer. *Nat Rev Urol* 2011; 8: 579–85

45 **Ho H, Yuen JS, Mohan P, Lim EW, Cheng CW.** Robotic transperineal prostate biopsy: pilot clinical study. *Urology* 2011; 78: 1203–8

46 **Cleary K, Melzer A, Watson V, Kronreif G, Stoianovici D.** Interventional robotic systems: Applications and technology state of the art. *Minim Invasive Ther Allied Technol* 2008; 15: 101–13

47 **Fütterer JJ, Barentsz JO.** MRI-guided and robotic-assisted prostate biopsy. *Curr Opin Urol* 2012; 22: 316–9

48 **Stoianovici D, Patriciu A, Mazilu D, Petrisor D, Kavoussi L.** A new type of motor: pneumatic step motor. *IEEE/ASME Trans Mechatron* 2007; 12: 98–106

49 **Lewin JS, Duerk JL, Jain VR, Petersilge CA, Chao CP, Haaga JR.** Needle localization in MR-guided biopsy and aspiration: effects of field strength, sequence design, and magnetic field orientation. *AJR Am J Roentgenol* 1996; 166: 1337–45

50 **Song SE, Cho NB, Iordachita II et al.** Biopsy needle artifact localization in MRI-guided robotic transrectal prostate intervention. *IEEE Trans Biomed Eng* 2012; 59: 1902–11

51 **Ukimura O, Desai MM, Palmer S et al.** 3-Dimensional elastic registration system of prostate biopsy location by real-time 3-dimensional transrectal ultrasound guidance with magnetic resonance/transrectal ultrasound image fusion. *J Urol* 2012; 187: 1080–6

52 **Pinkhasov GI, Lin YK, Palmerola R et al.** Complications following prostate needle biopsy requiring hospital admission or emergency department visits – experience from 1000 consecutive cases. *BJU Int* 2012; 110: 369–74

53 **Patel U, Dasgupta P, Amoroso P, Challacombe B, Pilcher J, Kirby R.** Infection after transrectal ultrasonography-guided prostate biopsy: increased relative risks after recent international travel or antibiotic use. *BJU Int* 2012; 109: 1781–5

54 **Sanders A, Buchan N.** Infection-related hospital admissions after transrectal biopsy of the prostate. *ANZ J Surg* 2013; 83: 246–8

55 **Symons JL, Huo A, Yuen CL et al.** Outcomes of transperineal template-guided prostate biopsy in 409 patients. *BJU Int* 2013; 112: 585–93

Correspondence: Govindarajan Srimathveeravalli, Department of Radiology Memorial Sloan-Kettering Cancer Center, H118 1275 York Ave, New York, NY 10065, USA.

e-mail: srimaths@mskcc.org

Abbreviations: PCa, prostate cancer; FOV, field of view: DoF, degrees of freedom; SNR, signal-to-noise ratio; NEX, number of excitations; TE, echo time; TR, repetition time; ST, slice thickness.